END

FILMED

DTIC

①

REPORT DOCUMENTATION PAGE	READ INSTRUCTIONS BEFORE COMPLETING FORM

1. REPORT NUMBER AFIT/CI/NR 85-94T	2. GOVT ACCESSION NO.	3. RECIPIENT'S CATALOG NUMBER

4. TITLE (and Subtitle) Mid-Range Spatial Frequency Errors In Optical Components	5. TYPE OF REPORT & PERIOD COVERED THESIS/DISSERTATION
	6. PERFORMING ORG. REPORT NUMBER

7. AUTHOR(s) Dale Kent Olinger	8. CONTRACT OR GRANT NUMBER(s)

9. PERFORMING ORGANIZATION NAME AND ADDRESS AFIT STUDENT AT: The University of Arizona	10. PROGRAM ELEMENT, PROJECT, TASK AREA & WORK UNIT NUMBERS

11. CONTROLLING OFFICE NAME AND ADDRESS AFIT/NR WPAFB OH 45433 - 6583	12. REPORT DATE 1983
	13. NUMBER OF PAGES 41

14. MONITORING AGENCY NAME & ADDRESS(if different from Controlling Office)	15. SECURITY CLASS. (of this report) UNCLASS
	15a. DECLASSIFICATION/DOWNGRADING SCHEDULE

16. DISTRIBUTION STATEMENT (of this Report)

APPROVED FOR PUBLIC RELEASE; DISTRIBUTION UNLIMITED

DTIC
ELECTE
AUG 16 1985
S
B
D

17. DISTRIBUTION STATEMENT (of the abstract entered in Block 20, if different from Report)

18. SUPPLEMENTARY NOTES

APPROVED FOR PUBLIC RELEASE: IAW AFR 190-1

LYNN E. WOLAVER
Dean for Research and
Professional Development
AFIT, Wright-Patterson AFB OH

19. KEY WORDS (Continue on reverse side if necessary and identify by block number)

20. ABSTRACT (Continue on reverse side if necessary and identify by block number)

ATTACHED

DD FORM 1473 EDITION OF 1 NOV 65 IS OBSOLETE

ABSTRACT

This research effort isolates a spatial frequency range of surface errors
of approximately two orders of magnitude neglected in standard optical
component specification and testing. The frequency range is bounded on the
low end by the Zernike Polynomial representation of the surface error function
and on the high end by root mean square surface roughness characterization.
These mid-range spatial frequencies are analyzed using a geometric optics
approach which predicts an out-of-focus intensity pattern containing
information directly related to the curvature errors present in the surface of
the optical component. The geometrical predictions provide the basis for a
proposed experimental technique for examining the mid-range spatial frequency
errors present in an optical component. The anticipated results and
observable errors using this technique are presented for an example component
and a discussion of extending this technique to other components is included.

AFIT RESEARCH ASSESSMENT

The purpose of this questionnaire is to ascertain the value and/or contribution of research accomplished by students or faculty of the Air Force Institute of Technology (AU). It would be greatly appreciated if you would complete the following questionnaire and return it to:

AFIT/NR
Wright-Patterson AFB OH 45433

RESEARCH TITLE: Mid-Range Spatial Frequency Errors In Optical Components

AUTHOR: Dale Kent Olinger

RESEARCH ASSESSMENT QUESTIONS:

1. Did this research contribute to a current Air Force project?

( ) a. YES   ( ) b. NO

2. Do you believe this research topic is significant enough that it would have been researched (or contracted) by your organization or another agency if AFIT had not?

( ) a. YES   ( ) b. NO

3. The benefits of AFIT research can often be expressed by the equivalent value that your agency achieved/received by virtue of AFIT performing the research. Can you estimate what this research would have cost if it had been accomplished under contract or if it had been done in-house in terms of manpower and/or dollars?

( ) a. MAN-YEARS _____   ( ) b. $_____

4. Often it is not possible to attach equivalent dollar values to research, although the results of the research may, in fact, be important. Whether or not you were able to establish an equivalent value for this research (3. above), what is your estimate of its significance?

( ) a. HIGHLY   ( ) b. SIGNIFICANT   ( ) c. SLIGHTLY   ( ) d. OF NO
     SIGNIFICANT   SIGNIFICANT   SIGNIFICANCE

5. AFIT welcomes any further comments you may have on the above questions, or any additional details concerning the current application, future potential, or other value of this research. Please use the bottom part of this questionnaire for your statement(s).

NAME   GRADE   POSITION

ORGANIZATION   LOCATION

STATEMENT(s):

MID-RANGE SPATIAL FREQUENCY ERRORS

IN OPTICAL COMPONENTS

by

Dale Kent Olinger

A Thesis Submitted to the Faculty of the

OPTICAL SCIENCES CENTER

In Partial Fulfillment of the Requirements
For the Degree of

MASTER OF SCIENCE

In the Graduate College

THE UNIVERSITY OF ARIZONA

1 9 8 3

STATEMENT BY AUTHOR

This thesis has been submitted in partial fulfillment of requirements for an advanced degree at The University of Arizona and is deposited in the University Library to be made available to borrowers under rules of the Library.

Brief quotations from this thesis are allowable without special permission, provided that accurate acknowledgment of source is made. Requests for permission for extended quotation from or reproduction of this manuscript in whole or in part may be granted by the head of the major department or the Dean of the Graduate College when in his judgment the proposed use of the material is in the interests of scholarship. In all other instances, however, permission must be obtained from the author.

SIGNED: *Dale Kent Olinger*

APPROVAL BY THESIS DIRECTOR

This thesis has been approved on the date shown below:

_____   _October 3, 1983_
R.E. PARKS   Date
Advisor

ACKNOWLEDGMENTS

This thesis is the culmination of a research effort undertaken under the suggestion and guidance of Robert E. Parks of the Optical Sciences Center, University of Arizona. The purpose of the project was to better define and take the first step in filling a void recognized for some time by Robert Parks in the field of optical component specification and testing. My sincere hope is that these efforts have at least set the proper course for filling this void and that I may have contributed in some small way toward mankind's knowledge and ability to live in peace and harmony with his universe.

To acknowledge the support and contributions of every one by name for the successful completion of this undertaking would be a disservice to those unintentionally left out. However, I must thank the U.S. Air Force for sponsoring my advanced education and providing the opportunity and privilege of participating in this academic community, the faculty and staff of the Optical Sciences Center, my fellow students, friends, and of course my family for their support in this venture. Special professional and personal thanks must be extended to my advisor, Robert E. Parks, for his patient guidance throughout the project; to the other members of my committee, Dr. Roland V. Shack and Dr. James C. Wyant, for their professional support; to J.H. Beckers and J.T. Williams whose internal memorandum served as the cornerstone upon which I was able to build, and finally

to Jeannette Gerl for her efforts in preparing the final document.
Personal acknowledgments go to my dear friend Kim Hunt whose friendship
allowed me to proceed with my degree, to my parents and in-laws for
their undying confidence, and most importantly to my wife Julie who
not only prepared the typed draft but also put up with me throughout
the course of my educational endeavor.   Finally, I would like to
dedicate this work to my wife, Julie, and my lovely daughter, Jennifer,
whose birth may have protracted the completion schedule for this thesis,
but the joy she brings is worth every minute of it.

TABLE OF CONTENTS

LIST OF TABLES

LIST OF ILLUSTRATIONS

ABSTRACT

This research effort isolates a spatial frequency range of surface errors of approximately two orders of magnitude neglected in standard optical component specification and testing. The frequency range is bounded on the low end by the Zernike Polynomial representation of the surface error function and on the high end by root mean square surface roughness characterization. These mid-range spatial frequencies are analyzed using a geometric optics approach which predicts an out-of-focus intensity pattern containing information directly related to the curvature errors present in the surface of the optical component. The geometrical predictions provide the basis for a proposed experimental technique for examining the mid-range spatial frequency errors present in an optical component. The anticipated results and observable errors using this technique are presented for an example component and a discussion of extending this technique to other components is included.

CHAPTER 1

INTRODUCTION

The evolution of optical component specification methods has led to the design, manufacture, and testing of optical components which must meet certain figure requirements, surface roughness limitations, and in some instances a less critical set of cosmetic specifications. Most common optical systems perform quite adequately when their components meet these design criteria.

The figure requirements for the optical component can be specified as an ideal surface figure equation and the allowed tolerances for deviation from that ideal figure. These tolerances are allocated during the design stage by establishing the desired image quality or other required system output, then evaluating the terms of the wavefront aberration function which would significantly impact that desired system output in order to set the acceptable upper bound for the coefficient of each term. The wavefront aberrations can be described in terms of the classical aberration functions; or alternatively, in the case of a circular pupil component, it is often convenient to use the Zernike polynomial expansion of the wavefront aberration function. For high quality optics applications, the Zernike coefficient tolerances may be specified to as many as 36 terms, which is a common limitation for the number of terms evaluated by interferogram analysis programs such as FRINGE (Loomis 1976, pp. 1 and 19). Using this method, the optical

1
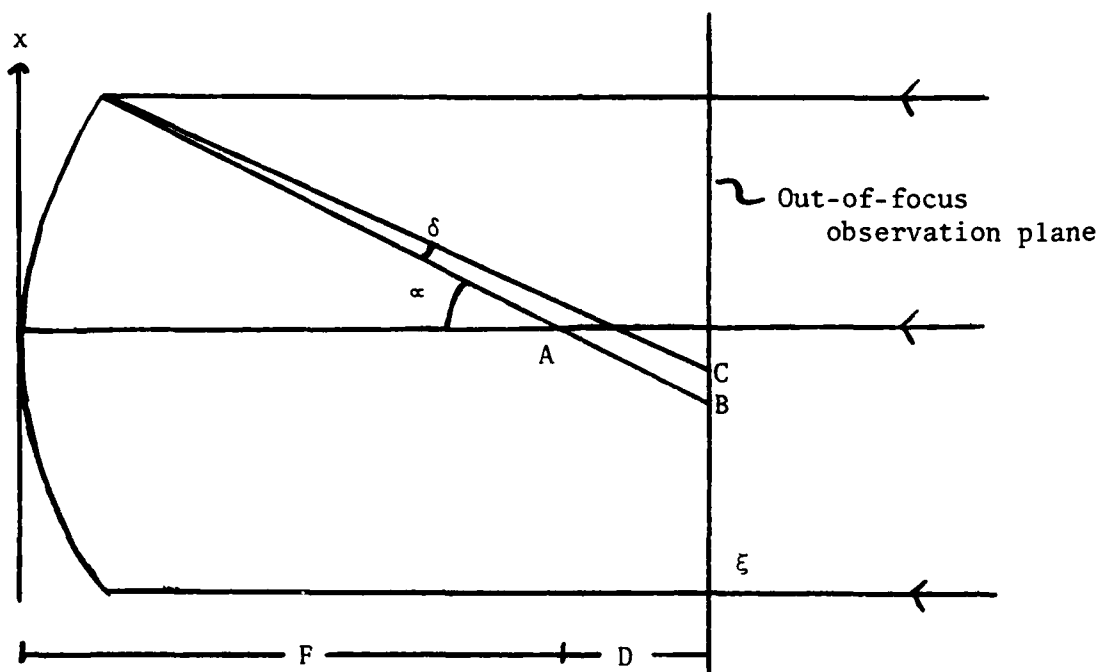
Figure 2. Optical Testing Geometry.

CHAPTER 3

A GEOMETRIC APPROACH TO EVALUATING
MID-RANGE SPATIAL FREQUENCIES

A geometrical examination of a perfect paraboloid will serve as the starting point for dealing with the mid-range spatial frequency errors in an optical element. The arrangement will be a uniform plane wave perpendicular to the optic axis illuminating a parabolic mirror as shown in Figure 2 (Beckers and Williams 1979).

For the perfect parabola, an incident ray entering the system will strike the mirror at a height x from the optic axis; cross the optic axis at the focal point A; and intersect the out-of-focus observation plane at point B, a height ξ from the optic axis. The equation governing the location of point B can be found using similar triangles as

$$\xi = x \frac{D}{F} \qquad (3-1)$$

where D is the distance from the focal plane to the out-of-focus observation plane and F is the focal length of the optical component.

If the surface of the optical element is now allowed to have slight imperfections, it will deviate from a perfect parabolic surface with a linear deviation

$$\Delta S = f(x) \qquad (3-2)$$

where $f(x)$ is the surface error as a function of the radial distance x. The slope error of the optical surface is simply given by the derivative

14

research for this paper and substantiated by Church, Howells and Vorburger (1981) who approached the problem only from an rms surface roughness standpoint. Direct extension of surface figure measurement and testing techniques seems to be of limited value in trying to bridge this gap. The extensive data sampling and analysis requirements needed to add additional polynomial terms to the low spatial frequency representation of the surface figure would be very burdensome, and as can be extrapolated from Table II the spatial frequency range does not expand very rapidly with additional terms. Mechanical surface roughness measurements are difficult to extend very far into the mid-range spatial frequency band because of the complications of trying to make precision measurements over longer pathlengths. These problems include thermal and electronic drift in the instruments, rejection of the desired sag for nonplanar components, the additional dynamic range required for nonplanar surfaces, the use of contact measurements over a long pathlength with the added potential for damage, and an increased requirement for environmental isolation during testing. Finally, scattering measurements are of limited value in bridging this gap since the low amplitude, mid-range spatial frequencies scatter light over very small angles which cannot be easily separated from the specular region. It is this slightly scattered light which may provide the basis for probing these mid-range spatial frequency errors.

$$d = \frac{\lambda}{\sin\theta_s} \qquad\qquad (2\text{-}5)$$

and an illuminating wavelength of 0.63 micrometers, the optical surface

spatial wavelengths spanned by such a measurement would be from 12 micro-

meters to 0.64 micrometers. Using a longer optical wavelength of

10.6 micrometers extends this range to spatial wavelengths from

200 micrometers to 10.6 micrometers. Using the widest possible spread

of spatial wavelengths from the above methods and an optical element

with a half meter diameter, the range covered by rms surface roughness

measurements is from 0.6 micrometers to 500 micrometers or in frequency

terms from 8.3×10^5 cycles per diameter to 1000 cycles per diameter.

The 1000 cycles per diameter figure will be adopted as an upper bound

to the mid-range spatial frequencies, even though this would vary with

the rms surface roughness measuring technique and the actual diameter

of the component under test.

The preceding paragraphs point to some potential problems that

can be encountered when specifying and purchasing an optical element

using standard specification techniques and draws a very rough boundary

around the bandwidth that has been called the mid-range spatial fre-

quencies in this paper. The cutoffs are somewhat arbitrary, but the

region from 5 to 1000 cycles per diameter needs to be better represented

in optical specification and testing of very high quality optical com-

ponents. This represents a bandwidth of better than two orders of

magnitude in the spatial frequency scale that is commonly disregarded.

There is a general lack of information in the literature related

to these mid-range spatial frequencies, as borne out by the preliminary

The characteristics of the high spatial frequency rms surface roughness must now be examined to arrive at an upper bound on the mid-range spatial frequency region. A number of methods are used to make surface roughness measurements; a few representative methods will be discussed to give a general indication of the spatial frequency bands included in an rms surface roughness measurement. It can be very misleading to rely on an rms surface roughness measurement without first knowing the range of frequencies included. Mechanical measurement of the surface contour with a finely pointed stylus is one common measuring technique. The inherent bandwidth limitations of this method involve the lateral resolution limits of the equipment from both electronic and mechanical filtering at the high frequency end and the linear scan length at the low frequency end. A recent article describes one such system with a horizontal resolution of 2 micrometers and a total linear scan length of 1500 micrometers (Bennett and Dancy 1981, p. 1786). This instrument will detect spatial wavelengths on the optical surface from 2 micrometers to 500 micrometers since there is a minimum factor of three reduction from the physical scan length to the detectable spatial wavelengths due to the sampling rates (Church, Howells and Vorburger 1981, p. 7). The second common method for determining rms surface roughness is the total integrated scatter (TIS) technique which measures the scattered intensity of normally incident light from near specular to near 90 degrees. The collecting optics require a range somewhat smaller than the full 90 degree sweep. A range from 3 to 85 degrees will be taken as a typical arrangement (Church, Howells and Vorburger 1981, p. 3). Using the normal incidence grating equation

Table II. Bessel Function Zeros

Zernike index n	Corresponding Bessel function index	First zero of Bessel function(x)	Spatial frequency at first zero $\left(\dfrac{x}{\pi}\right)$ in $\dfrac{\text{cycles}}{\text{diameter}}$
0	1	3.8	1.2
1	2	5.1	1.6
2	3	6.4	2.0
3	4	7.6	2.4
4	5	8.8	2.8
5	6	9.9	3.2
6	7	11.1	3.5
7	8	12.2	3.9
8	9	13.4	4.3
9	10	14.5	4.6
10	11	15.6	5.0
11	12	16.7	5.3
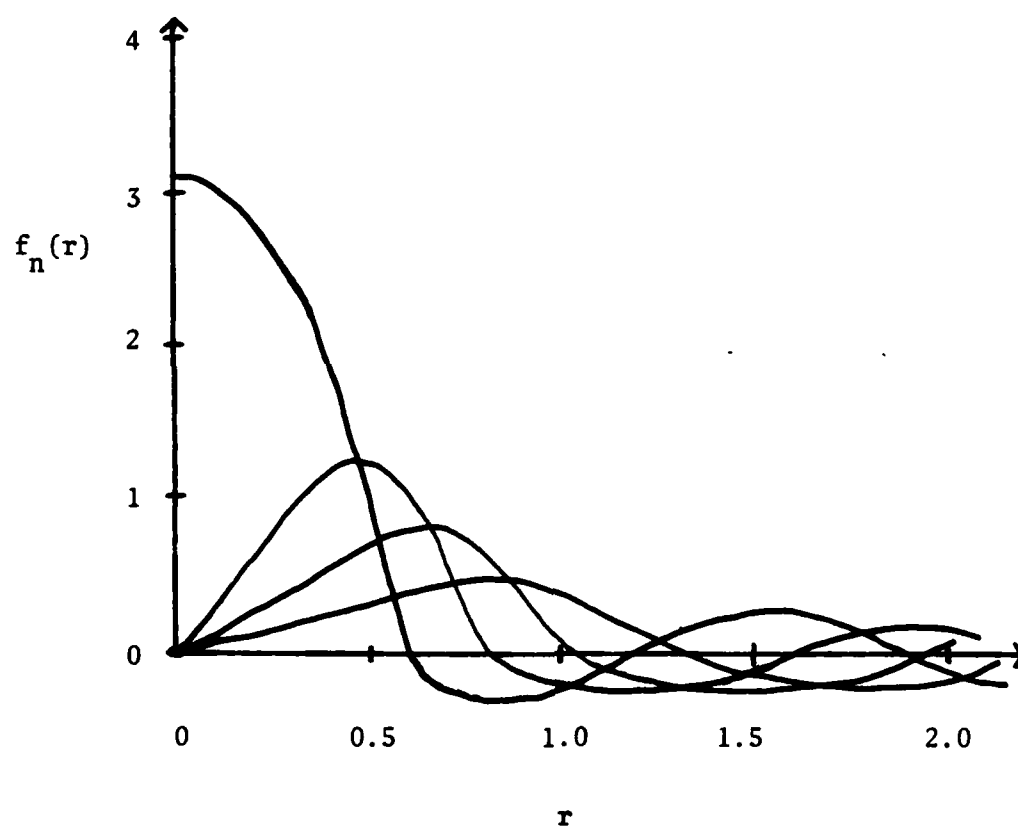
Figure 1. First Four Zernike Spatial Frequency
Functions (Equation 2-3).

order $n+1$ where n is the Zernike polynomial index (see Table I). Kintner and Sillitto (1976, p. 610) plotted the results for the first several functions

$$f_n(r) = 2\pi \frac{J_{n+1}(2\pi r)}{2\pi r} \qquad (2-3)$$

and this graph is shown in Figure 1. As shown by the graph of these functions, there is no true cutoff frequency for a given Zernike term; however, choosing the first zero crossing of the Bessel function related to each term can serve as a representative limit beyond which the spatial frequencies are at least poorly represented in the Zernike polynomial expansion through that term. The Bessel function is represented by an infinite series

$$J_n(x) = \sum_{k=0}^{\infty} \frac{(-1)^k}{k!\Gamma(n+k+1)} \left(\frac{x}{2}\right)^{n+2k} \qquad (2-4)$$

(Selby 1972, p. 518). A program for the TI Programmable 58C/59 Calculator was written to evaluate this function and has been included as Appendix A. The first zero for each Bessel function through the twelfth order was calculated using this program and is displayed in Table II. Examining the data in this table shows that the spatial frequencies well represented by even the first 36 terms of the Zernike polynomial span the very limited range from approximately zero to five cycles per diameter using the first zero criteria. Since there is no true cutoff frequency, five cycles per diameter will be selected as the representative upper bound for the low spatial frequency description of an optical component.

Table I.   Zernike Polynomials

#	n	$\lvert m\rvert$	Polynomial Term
0	0	0	1
1	1	1	$\rho \cos\phi$
2	1	1	$\rho \sin\phi$
3	2	0	$2\rho^2 - 1$
4	2	2	$\rho^2 \cos2\phi$
5	2	2	$\rho^2 \sin2\phi$
6	3	1	$(3\rho^2 - 2)\rho \cos\phi$
7	3	1	$(3\rho^2 - 2)\rho \sin\phi$
8	4	0	$6\rho^4 - 6\rho^2 + 1$
9	3		$\rho^3 \cos3\phi$
10	3		$\rho^3 \sin3\phi$
11	4	2	$(4\rho^2 - 3)\rho^2 \cos2\phi$
12	4	2	$(4\rho^2 - 3)\rho^2 \sin2\phi$
13	5	1	$(10\rho^4 - 12\rho^2 + 3)\rho \cos\phi$
14	5	1	$(10\rho^4 - 12\rho^2 + 3)\rho \sin\phi$
15	6	0	$20\rho^6 - 30\rho^4 + 12\rho^2 - 1$
16	4	4	$\rho^4 \cos4\phi$
17	4	4	$\rho^4 \sin4\phi$
18	5	3	$(5\rho^2 - 4)\rho^3 \cos3\phi$
19	5	3	$(5\rho^2 - 4)\rho^3 \sin3\phi$
20	6	2	$(15\rho^4 - 20\rho^2 + 6)\rho^2 \cos2\phi$
21	6	2	$(15\rho^4 - 20\rho^2 + 6)\rho^2 \cos2\phi$
22	7	1	$(35\rho^6 - 60\rho^4 + 30\rho^2 - 4)\rho \cos\phi$
23	7	1	$(35\rho^6 - 60\rho^4 + 30\rho^2 - 4)\rho \sin\phi$
24	8	0	$70\rho^8 - 140\rho^6 + 90\rho^4 - 20\rho^2 + 1$
25	5	5	$\rho^5 \cos5\phi$
26	5	5	$\rho^5 \sin5\phi$
27	6	4	$(6\rho^2 - 5)\rho^4 \cos4\phi$
28	6	4	$(6\rho^2 - 5)\rho^4 \sin4\phi$
29	7	3	$(21\rho^4 - 30\rho^2 + 10)\rho^3 \cos3\phi$
30	7	3	$(21\rho^4 - 30\rho^2 + 10)\rho^3 \sin3\phi$
31	8	2	$(56\rho^6 - 105\rho^4 + 60\rho^2 - 10)\rho^2 \cos2\phi$
32	8	2	$(56\rho^6 - 105\rho^4 + 60\rho^2 - 10)\rho^2 \sin2\phi$
33	9	1	$(126\rho^8 - 280\rho^6 + 210\rho^4 - 60\rho^2 + 5)\rho \cos\phi$
34	9	1	$(126\rho^8 - 280\rho^6 + 210\rho^4 - 60\rho^2 + 5)\rho \sin\phi$
35	10	0	$252\rho^{10} - 630\rho^8 + 560\rho^6 - 210\rho^4 + 30\rho^2 - 1$
36	6	0	$924\rho^{12} - 2772\rho^{10} + 3150\rho^8 - 1680\rho^6 + 420\rho^4 - 42\rho^2 + 1$

where n and m are integers; $n \geq 0$, $|m| \leq n$; and $\frac{n+m}{2}$ is an integer (Born and Wolf 1965, p. 464; Kintner and Sillitto 1976, p. 608). The series of functions $R_n^m(\rho)$ describe the radial variation across the pupil. These are then combined with the angular functions as indicated to complete the description of the pupil function. Equation 2-1 can also be represented in terms of the real angular functions. The first 36 terms of this polynomial as used by the FRINGE interferogram reduction program are listed in Table I along with their polynomial indexes n and m (Loomis 1976, p. 37). The FRINGE program selected the Zernike polynomial representation based on its orthogonal properties and is capable of reducing an interferogram's fringe pattern to its representative Zernike coefficient for up to the first 36 terms employing a Gram-Schmidt least squares procedure (Loomis 1976, p. 1). The limitation of 36 terms is somewhat arbitrary but is a fairly common choice for the useful number of polynomial terms due to the noise present in the fringe pattern and the additional computations required to extend beyond 36 terms.

The reason for selecting the Zernike representation for the low spatial frequency description in this case is that the Fourier transform will help illuminate the spatial frequencies represented by such a description. Kintner and Sillitto (1976, p. 610) show that the transform of each term of the Zernike polynomial is

$$F\{V_n^m(\rho,\phi)\} \equiv V_n^m(r,\theta) = 2\pi(-i)^n \frac{J_{n+1}(2\pi r)}{2\pi r} e^{im\theta}, \qquad (2\text{-}2)$$

where $J_n(x)$ represents the Bessel function.

Examination of equation 2-2 indicates the radial spatial frequency range of each Zernike term is governed by the Bessel function of

degraded propagation qualities. Another cause for concern when over-looking the effects of these mid-range spatial frequency errors is the introduction of new optical manufacturing techniques which can inherently create significant errors within this region. Standard specification and testing procedures would then prove inadequate to avoid and/or detect the presence of those errors. Numerically controlled generation of optical surfaces, such as single point diamond turning, will produce periodic surface errors over a wide range of spatial frequencies. Many of these errors are not readily removed even during subsequent polishing which is intended to remove the apparent tooling marks. Localized and numerically controlled polishing operations are additional recently introduced manu-facturing techniques which could be plagued by mid-range spatial fre-quency effects. These are just a few examples where this overlooked region of optical specification and testing could result in adverse and surprising impacts on overall system performance.

The next requirement is to better define this mid-range spatial frequency range, which must be accomplished by first examining the spatial frequency ranges covered by conventional optical specification and testing methods.

The low spatial frequency range can be discussed in terms of the Zernike polynomial expansion of the pupil function of an optical element. Born and Wolf show that the pupil function over a unit circle can be characterized by the complete and orthogonal set of Zernike polynomial functions

$$V_n^m(\rho,\phi) = R_n^m(\rho)\, e^{im\phi}; \qquad\qquad (2-1)$$

CHAPTER 2

BACKGROUND AND DEFINITION OF MID-RANGE
SPATIAL FREQUENCIES

The impetus for this investigation came from an internal memorandum from the Multiple Mirror Telescope Observatory (Beckers and Williams 1979) regarding the observance of inexplicable ringlike intensity variations in out-of-focus images obtained from the multiple mirror telescope (MMT). Edge diffraction within the optical train was experimentally ruled out as the source of this modulation, leading to the speculation that the phenomenon could be attributed to zonal variations in the primary mirror system of the MMT. Modeling the primary using the mid-range spatial frequency hypothesis and geometric analysis as presented in Chapter 3 led to a very plausible explanation for the source of these intensity variations in the out-of-focus images.

This memorandum pointed toward a broader examination of areas where these mid-range spatial frequency errors may need to be considered in the design, specification, manufacture, and testing of various optical components. Such errors could manifest themselves as loss of signal in weak signal applications, as false structure or image degradation in high resolution astronomical telescopes or other high resolution imaging systems, as parasitics in high power laser resonators, or as stray or lost energy within high power beams. The resultant energy redistribution within high energy systems could cause destructive power loadings and

bearing on the actual performance. This specification is commonly referred to as scratch-dig and identifies the acceptable number and size of defects observable to the human eye. Applications where these defects can be detrimental to system performance, rather than simply an aesthetic quality factor, do occur when a component is located near a focal plane or in a high power system where localized defects could lead to destructive levels of absorption or scattering. This specification is difficult to characterize in terms of the spatial frequency spectrum due to the localized nature of the defects and in high quality applications scratches and digs are usually unacceptable. Therefore, this specification will not be discussed further.

The requirements of most optical systems are met quite satisfactorily using just the above, well-established, design criteria. On the other hand, these specification criteria leave a significant range of spatial frequencies underrepresented or completely overlooked in the commonly accepted methods of specifying and testing optical components. These overlooked spatial frequencies can still cause undesirable effects in optical systems requiring very high quality. It is this spatial frequency range which will form the basis for this analysis and will be referred to as the mid-range spatial frequencies. This analysis may lead the way to bridging a significant region of this gap in optical component specification and testing.

component can be manufactured and then checked interferometrically to verify compliance with the specified figure requirements. However, as will be shown in Chapter 2, figure requirements specified through even the first 36 terms of the Zernike polynomial primarily deal with spatial frequencies from about zero to five cycles per diameter of the optical component.

On the opposite end of the spatial frequency scale from the figure requirements lies the surface roughness description of the optical component. The primary impact of surface roughness on the performance of an optical system is in the form of scattering. An optical component could conceivably meet surface figure specifications while still producing a very poor quality image or excessive signal losses due to surface roughness. To avoid this situation, an acceptable root mean square (rms) surface roughness tolerance is commonly specified which will prescribe the specular versus diffuse properties of the optical surface. Several methods have been developed for testing and analyzing surface roughness, including direct surface contour measurement with a mechanical stylus probe and various light scattering and reflection techniques. These measurement techniques have inherent spatial frequency limitations which will be discussed in further detail in Chapter 2. In general, the spatial wavelengths covered by the rms surface roughness description are from about 0.6 micrometers to 500 micrometers, which for a half meter diameter component represents a spatial frequency range from 8.3×10^5 cycles per diameter to 1000 cycles per diameter.

The third specification type mentioned was the cosmetic appearance of an optical component, which under most applications has little

of the surface error function

$$\Delta\Phi = \frac{d\ f(x)}{dx} \qquad\qquad (3\text{-}3).$$

The incoming object ray will experience an angular deviation from its

geometric path for a perfect parabola of twice the surface slope error or

$$\delta(x) = 2\ \frac{d\ f(x)}{dx} \qquad\qquad (3\text{-}4).$$

The intersection of this deviated ray with the out-of-focus observation

plane will then become

$$\xi' = x\ \frac{D}{F} + \delta(x)\ \frac{F+D}{\cos(\alpha-\delta)} \qquad\qquad (3\text{-}5).$$

If the angle $\alpha-\delta$ is held to a very small angle where $\cos(\alpha-\delta) \approx 1$ (which

would restrict the use of the following equation for small F number

systems to the paraxial region and requires that the surface slope

errors are not too extreme), then equation 3-5 can be approximated as

$$\xi' \approx x\ \frac{D}{F} + \delta(x)(F+D) \qquad\qquad (3\text{-}6).$$

Requiring that the slope error be small in magnitude is consistent with

the fact that only very high quality optics are being considered when

mid-range spatial frequencies are being considered.

If the illuminating plane wave has a uniform intensity I_o, the

intensity pattern in the out-of-focus observation plane would have a

geometrically predicted structure of

$$i(\xi') = I_o\ \frac{dx}{d\xi'} \qquad\qquad (3\text{-}7)$$

$$= I_o \left[\frac{D}{F} + \frac{d\ \delta(x)}{dx}\ (F+D) \right]^{-1} \qquad\qquad (3\text{-}8)$$

$$= I_o \left(\frac{F}{D}\right) \left[1 + \frac{d\ \delta(x)}{dx}\ \frac{(F+D)F}{D} \right]^{-1} \qquad\qquad (3\text{-}9).$$

Using a binomial expansion of the term in square brackets and the fact that $\delta(x)$ was assumed to be a small and well bounded function, equation 3-9 can be rewritten as

$$i(\xi') = I_o \left(\frac{F}{D}\right) \left\{ 1 - \frac{d\ \delta(x)}{dx}\ \frac{(F+D)F}{D} + \left[\frac{d\ \delta(x)}{dx}\ \frac{(F+D)F}{D}\right]^2 - \cdots \right\}$$

(3-10)

or

$$i(\xi') \simeq I_o \left(\frac{F}{D}\right) \left[1 - \frac{d\ \delta(x)}{dx}\ \frac{(F+D)F}{D}\right]$$

(3-11).

Defining the nominal intensity level as

$$i_o \equiv I_o \left(\frac{F}{D}\right)$$

(3-12)

and using the results of equation 3-4, equation 3-11 can now be written as

$$i(\xi') = i_o \left[1 - 2\ \frac{d^2\ f(x)}{dx^2}\ \frac{(F+D)F}{D}\right]$$

(3-13).

This equation then predicts the intensity modulation in the out-of-focus observation plane to be proportional to the second derivative of the surface error function of equation 3-2, which represents the curvature error of the optical surface. This is conceptually pleasing since a curvature error in the optical surface would be expected to lead to regional focal length changes and therefore intensity fluctuations. For example, a region of greater curvature than desired would have a shorter focal length causing a brighter region on the short side of nominal focus and a less intense region on the opposite side of focus. Equation 3-13 also predicts this contrast reversal that would be expected on opposite sides of focus. The intensity modulation is also shown to vary inversely with the distance the observation plane is from

the focal plane. With this in mind, it is reasonable to choose an observation plane where $F \gg D$ so that equation 3-13 can be rewritten as

$$\dot{\iota}(\xi') = \dot{\iota}_o \left[1 - 2 \frac{d^2 f(x)}{dx^2} \left(\frac{F^2}{D}\right) \right] \tag{3-14}.$$

While the preceding paragraph indicates that D must be much less than F to maximize the intensity modulation, several problems arise when the observation plane is located too close to the focal plane. The first problem is that when D becomes too small the approximation made in proceeding from equation 3-10 to equation 3-11 is violated. The point where this restriction is violated is dependent upon the magnitude of the surface curvature error, as well as the focal length of the optical component. A second practical problem is that, even relying on geometric analysis near the focal region, one would find the resultant intensity pattern too small to properly observe and analyze. One final point is that, near the focal plane, geometric analysis of an arrangement such as depicted in Figure 2 is inadequate and the region would be dominated by diffraction effects which are beyond the scope of this paper. This final restriction will be assumed to require that the observation plane be outside the depth of focus or

$$D \gg \lambda \text{ (F-number)}^2 \tag{3-15}.$$

To further describe what would be expected from an optical surface, the surface error function can be represented as a Fourier series with angular frequency

$$\omega = \frac{2\pi}{L} \tag{3-16}$$

where L is the spatial wavelength of the surface error. The surface

error function is then represented by

$$f(x) = \sum_n \left[A_n \cos\omega_n x + B_n \sin\omega_n x \right] \qquad (3\text{-}17)$$

which has its second derivative

$$\frac{d^2 f(x)}{dx^2} = \sum_n \left[-A_n \omega_n{}^2 \cos\omega_n x - B_n \omega_n{}^2 \sin\omega_n x \right] \qquad (3\text{-}18).$$

The contribution of each term of the Fourier series to the intensity pattern as described by equation 3-14 is then

$$i(\xi') = i_o \left[1 - 2A_n \omega_n{}^2 \left(\frac{F^2}{D}\right) \cos\omega_n x - 2B_n \omega_n{}^2 \left(\frac{F^2}{D}\right) \sin\omega_n x \right]$$

$$(3\text{-}19).$$

The effect is therefore weighted by the square of the spatial frequency and linearly with the amplitude of the error.

One final conceptual barrier must be crossed before the geometric theory presented could be applied. As previously mentioned, diffraction effects would predominate at least in the focal region. They are still present even outside this region and must be dealt with in some fashion. Since an analytic description of the diffraction effects is beyond the scope of this paper, the diffraction effects will be treated conceptually. The diffraction pattern from the surface will be treated as if it were superimposed over the geometrically predicted intensity pattern. Malacara (1978, pp. 356-359) describes the diffraction intensity distribution on either side of the focal plane and presents a diagram of the intensity pattern. This intensity pattern is symmetric about the focal plane and may be the key to overcoming diffraction effects in any analysis undertaken using the geometric theory presented. Since the geometrically predicted pattern undergoes a contrast reversal upon

passing through the focal plane, a set of two intensity patterns obtained from observation planes located on opposite sides but at equal distances from the focal plane would allow the removal of the overlying diffraction pattern.

The intensity pattern derivation presented in this chapter is based upon and borrows extensively from a similar derivation outlined in the MMT memorandum authored by J.M. Beckers and J.T. Williams mentioned at the beginning of Chapter 2 (Beckers and Williams 1979). The purpose of that memorandum was to present a possible explanation for a phenomenon observed while viewing with the MMT. The intent of this paper is to expand this phenomenon description into a proposed technique for evaluating optical components in hopes of bridging at least part of the spatial frequency gap that currently exists in optical testing.

CHAPTER 4

ANALYSIS OF MID-RANGE SPATIAL FREQUENCIES USING THE OUT-OF-FOCUS INTENSITY DISTRIBUTION

The preceding chapter developed an analytical tool which must now be evaluated for its potential to fill in the mid-range spatial frequency gap in optical testing. The basic procedure would be to illuminate the component being tested with a uniform intensity plane wave, bring the component's output to focus, and then examine the intensity distribution in an out-of-focus observation plane either inside or outside the focal plane. This intensity distribution would be spectrally analyzed to provide the information required to evaluate the spatial frequency errors present in the optical component. This chapter will discuss some of the aspects of actually performing this type of test and show the results anticipated.

The first consideration in performing an actual test is to select an illumination source. The required output of the source is a uniform intensity plane wave. A collimated laser source as commonly employed in optical testing is probably inappropriate for this arrangement. The monochromatic, coherent nature of the laser source would lead to a speckle pattern in the observation plane, making analysis of the intensity pattern difficult and possibly misleading. Therefore, a near point source of white light placed at the focus of a high quality parabola would be the primary choice for producing the desired plane

wave. The absolute source intensity does not present a significant
problem, even when considering such a small primary source, since it is
the modulation of the resultant intensity pattern in the out-of-focus
observation plane which provides the necessary information. A white
light source, rather than a filtered source, was selected by con-
sidering the available intensity and the prospect of washing out some
of the undesirable diffraction effects that would cause intensity
variations of their own in the observation plane. These diffraction
effects would still be present using a white light source, but they
are wavelength dependent; whereas, the predicted geometric slope
errors caused by the surface errors of the component would be wave-
length independent. The final source plane wave intensity profile must
be scanned for uniformity before any additional testing.

This discussion will now be restricted to focusing reflective
elements. Nonfocusing elements would require auxillary optics and
refractive elements lead to additional wavelength considerations. The
axis of the optical element which will be tested should be aligned
perpendicular to the illuminating plane wavefront so that it then brings
the wavefront to a sharp focus. Testing of nonparabolic surfaces
introduces inherent intensity distributions which must be accounted for
prior to analyzing the out-of-focus intensity pattern for the mid-range
spatial frequencies present.

Now that the optical component is focusing the incident plane
wave, actually employing the equations developed in Chapter 3 is
dependent on knowing the exact focal length and accurately positioning
the out-of-focus observation plane relative to the focal plane. The

paraxial focal plane can be identified very accurately using a simple

knife edge test. The focal length can then be measured to this focal

plane with great precision using a distance measuring interferometer.

The observation planes both insdie and outside of this focal plane

can then be selected and positioned to this same level of precision.

This positioning becomes even more critical if an attempt is made to

compare the intensity profiles from inside and outside of focus to

confirm the expected contrast reversal or if trying to remove the

diffraction effects as discussed previously.

Once the out-of-focus observation plane has been selected and

located, the next task is to record the intensity profiles found in

those planes. At least three possible methods exist for performing

this task, each with its own advantages and disadvantages. The first

method would be to photograph the intensity pattern for subsequent

development and then analysis with a microdensitometer. The second

method would be to scan the intensity profile with a fiber optic probe.

The final method that will be discussed would be to use a charge coupled

device (CCD) array for recording the intensity profiles.

Photographing the out-of-focus intensity pattern provides a

visual permanent record that is an appropriate medium for verifying the

existence of the mid-range spatial frequency effects. Such photographs

do exist for the MMT showing a very marked radial structure to the

intensity profile (Beckers and Williams 1979), but the reproductions are

of very poor quality and the data are incomplete for actually performing

an analysis. However, the existence of this phenomenon in the MMT was

not only the impetus for this investigation as earlier indicated, it

lends credence to using such an intensity pattern to evaluate the surface errors. Photographing the intensity patterns can go beyond simple verification. The film selected must have a film grain size small enough to avoid spatially integrating the intensity pattern details representing the mid-range spatial frequency errors to be analyzed, as well as possessing a dynamic range capable of recording the anticipated intensity modulations. Once the pattern has been recorded and the film is developed, a microdensitometer can be used to provide the radial intensity profiles for spectral analysis to determine their spatial frequency content. Combinations of film characteristics and microdensitometer capabilities are available that can record spatial wavelengths as small as 20 micrometers (Kodak 1973; Joyce Instrumentation 1963), as measured in the plane of the photograph. This method has several significant advantages in addition to the permanent visual record. The data are recorded for the entire observation region over a very short period of time, minimizing environmental isolation and drift problems. The microdensitometer tracings can be performed away from the laboratory test environment and the automation of the microdensitometer makes it easy to compile several radial scans for statistical comparison. The primary drawback to photographic recording is the presence of a large central obscuration in the test setup or the requirement to use the optical component off axis to avoid such an obscuration. The selection of the preferable alternative depends on the nature of the component under test. One used with a central obscuration can be tested with a similar obscuration, while a component used off axis should be tested as such. Additional problems encountered in the use of

photographic recording are the variable sensitivity of the film to
different optical wavelengths, the rapid modulation transfer function
dropoff with increasing spatial frequency, and the film's limited
ability to record the lower level intensity modulations.

The second potential method for recording the out-of-focus
intensity profile is to use a very small diameter fiber optic probe
scanned across the radius of the pattern. This intensity profile must
then be recorded for later spectral analysis. Optical fibers are
available for use as such a probe with core diameters smaller than
10 micrometers (Levitt 1982) which could provide information on spatial
wavelengths in the observation plane to as small as 20 micrometers.
This is on the same order as the photographic capabilities, but the
use of a fiber optic probe eliminates the need to test off axis and
minimizes any obscuration of the component under test. There are some
significant drawbacks to the use of a fiber optic probe. The primary
difficulty is the requirement to design and construct a radial scan
mechanism that would keep the probe in a single plane perpendicular to
the optic axis with minimal vibration. This method also substantially
increases the time needed for data accumulation in the test setup making
environmental isolation more critical. Advantages of this method in
addition to the removal of a major central obscuration include the
availability of detectors with fairly linear response to a wide range of
optical wavelengths, direct data readout of the radial scans allowing
signal processing, and control over the scan rate permitting adjustments
to various signal intensities.

The final option that should be evaluated is the use of a linear CCD array to provide an immediate readout of a radial scan of the intensity profile. This method is intermediate between the other two in terms of obscuration or off axis requirements during testing. Linear CCD arrays, such as the Reticon G series, are readily available with detector spacings of 25 micrometers center to center and a fairly linear response over the visible wavelength region, allowing evaluation of spatial wavelengths in the observation plane as small as 50 micrometers (Reticon 1976). CCD arrays have also been made with resolutions of 33 lines per millimeter (Howes and Morgan 1979, p. 250) which would provide information on spatial wavelengths to 30 micrometers. Use of a CCD array would allow very rapid data accumulation and readout, making it comparable in speed to the photographic method, except that repeated radial scans would require repositioning of the array and retesting of the element. The CCD array has the advantage over the fiber optic probe in that it does not require scanning across the radius to accumulate data, while still providing the variable integration time feature. CCD arrays also provide a sizable dynamic range.

Selection between these three methods would depend upon availability, cost, and experimental verification of the technique. Photographic recording would be the most appropriate choice to provide the experimental verification that this testing technique for evaluating mid-range spatial frequencies is viable. The photograph allows the experimenter more flexibility in selecting the radial profiles to analyze and provides more direct feedback over the entire observation plane. This could prove very beneficial when trying to observe and

analyze other effects that may be complicating or overriding the predicted intensity modulation. After validation of the basic method, the CCD array would probably prove to be the best method for component evaluation by virtue of its speed and data output capabilities. The advantages that could make the fiber optic probe most useful under certain testing requirements would be that it could have the highest resolution if one of the thinnest optical fibers manufactured is compatible with this application and the fact that it creates the least obscuration.

While each of these recording methods has its own advantages and disadvantages, they all suffer from a common set of testing problems. Vibration isolation would be very crucial, and the longer the test and integration times the more stringent the requirements would be. Background illumination would have to be suppressed as much as possible in all three methods to preclude reducing the modulation intensity. The analysis presented in Chapter 3 dealt only with radial spatial frequencies. For components with angular errors, there would also be an angular intensity modulation, requiring more detailed analysis or many radial scans at various locations to provide adequate statistics. Diffraction effects have already been mentioned at the end of Chapter 3 along with a possible method of dealing with them. The diffraction effects are symmetric about the focal plane, while the mid-range spatial frequency intensity modulations have been predicted to reverse contrast on either side of focus. The effects actually observed in the case of the MMT did show this contrast reversal (Beckers and Williams 1979, p. 3). One final problem associated with this testing

procedure would be attempting to correlate the magnitude of the intensity modulation measured in the observation plane to the amplitude of the corresponding surface error in the component being tested. This problem arises from the approximations made in developing the predicted intensity pattern, the nonlinearities during detection and analysis of the intensity pattern, and the various noise sources that have been mentioned.

To demonstrate the validity of pursuing this testing method for examining the mid-range spatial frequency errors of an optical component, an example component will be evaluated to show the anticipated results. The example component will be a half meter diameter, f/5 parabolic primary mirror intended for high resolution imagery. This mirror would have a 2.5-meter focal length and will be examined at out-of-focus observation planes both 5 percent and 10 percent of the focal length from the focal plane. Equation 3-19 provides the predicted radial profile of the intensity pattern. Assuming symmetry about the optic axis to examine the intensity modulation expected to be observable, equation 3-19 can be reduced to only the even function modulation terms where

$$i(\xi') = i_o \left[1 - 2A_n\omega_n^2 \left(\frac{F^2}{D}\right) \cos\omega_n x \right] \tag{4-1}$$

where ω_n is defined by equation 3-16. The modulation of the intensity pattern expressed as a percentage of the average intensity can then be expressed as

$$M = (100) \ 2A_n\omega_n^2 \left(\frac{F^2}{D}\right) \cos\omega_n x \tag{4-2}.$$

If the detection method selected can record a modulation of a given

percentage, then the minimum amplitude of the error observable at a spatial frequency ω_n is

$$A_n = \frac{(0.01)\ M}{2\omega_n^2} \left(\frac{D}{F^2}\right) = \frac{(0.01)\ ML^2}{8\pi^2} \left(\frac{D}{F^2}\right) \qquad (4\text{-}3),$$

where in this example component D is either 5 or 10 percent of the focal length, F; and L is varied to span the mid-range spatial frequencies. Table III lists the minimum amplitude, A_n, of the errors on the optical surface of the half meter parabola that would be observable as an intensity modulation in an observation plane 10 percent of the focal length from the focal plane. Detectable modulation levels of 50, 25, 10, and 5 percent have been included in the table. Table IV presents the same set of data for the half meter parabola except the out-of-focus observation plane is located only 5 percent of the focal length from the focal plane.

The data in Table III have been presented graphically on a log-log scale in Figure 3 and Table IV has been presented in the same manner in Figure 4. Also shown in Figures 3 and 4 are the limits of the mid-range spatial frequency region as defined in Chapter 2 for a half meter diameter component. Spatial frequencies greater than 1000 cycles per diameter can be evaluated using an rms surface roughness measurement of the optical component, and spatial frequencies at least to 5 cycles per diameter can be evaluated interferometrically and represented by the Zernike polynomial coefficients. The two lines at the top of the graph represent surface errors with amplitudes of a quarter wave and an eighth wave of 600 nanometer wavelength light.

Table III. Amplitude of Minimum Observable Surface Error
at 10% Out-of-focus (0.5 m, f/5 parabola)

Spatial frequency (cycles/diameter)	Surface wavelength (mm)	A_n (nm) for detectable modulations			
		50%	25%	10%	5%
5	100.0	2530.0	1270.0	507.0	253.0
10	50.0	633.0	317.0	127.0	63.3
15	33.3	281.0	141.0	56.3	28.1
20	25.0	158.0	79.2	31.7	15.8
25	20.0	101.0	50.7	20.3	10.1
50	10.0	25.3	12.7	5.07	2.53
75	6.67	11.3	5.63	2.25	1.13
100	5.00	6.33	3.17	1.27	0.633
150	3.33	2.81	1.41	0.563	0.281
200	2.50	1.58	0.792	0.317	0.158
250	2.00	1.01	0.507	0.203	0.101
500	1.00	0.253	0.127	0.051	0.025
750	0.667	0.113	0.056	0.023	0.011
1000	0.500	0.063	0.032	0.013	0.006
1500	0.333	0.028	0.014	0.006	0.003
2000	0.250	0.016	0.008	0.003	0.002
2500	0.200	0.010	0.005	0.002	0.001

Table IV. Amplitude of Minimum Observable Surface Error
at 5% Out-of-focus (0.5 m, f/5 parabola)

Spatial frequency (cycles/diameter)	Surface wavelength (mm)	A_n (nm) for detectable modulations			
		50%	25%	10%	5%
5	100.0	1270.0	633.0	253.0	127.0
10	50.0	317.0	158.0	63.3	31.7
15	33.3	141.0	70.4	28.1	14.1
20	25.0	79.2	39.6	15.8	7.92
25	20.0	50.7	25.3	10.1	5.07
50	10.0	12.7	6.33	2.53	1.27
75	6.67	5.63	2.81	1.13	0.563
100	5.00	3.17	1.58	0.633	0.317
150	3.33	1.41	0.704	0.281	0.141
200	2.50	0.792	0.396	0.158	0.079
250	2.00	0.507	0.253	0.101	0.051
500	1.00	0.127	0.063	0.025	0.013
750	0.667	0.056	0.028	0.011	0.006
1000	0.500	0.032	0.016	0.006	0.003
1500	0.333	0.014	0.007	0.003	0.001
2000	0.250	0.008	0.004	0.002	0.001
2500	0.200	0.005	0.003	0.001	0.001
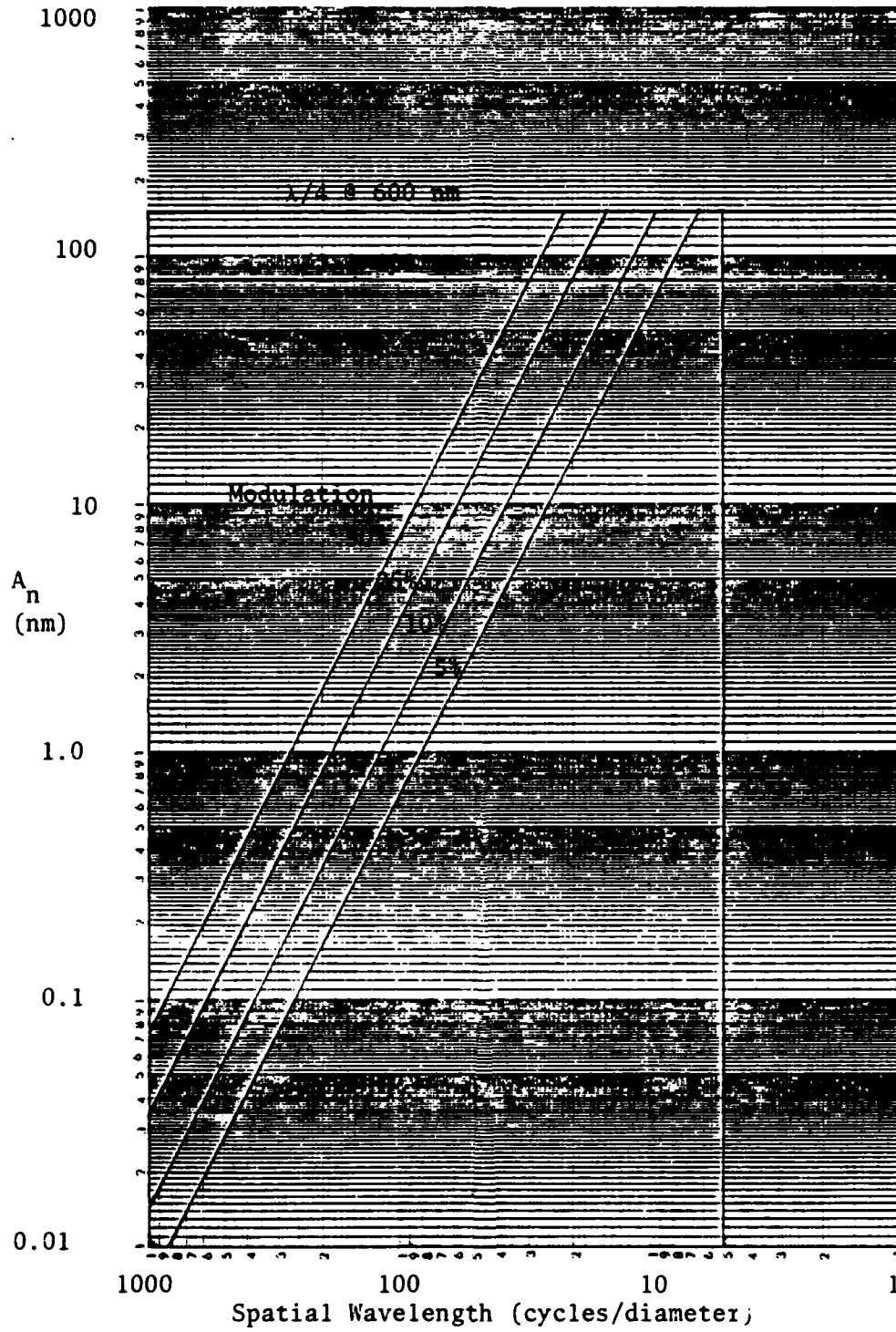
Figure 3. Detectable Amplitudes at 10% Out-of-Focus.
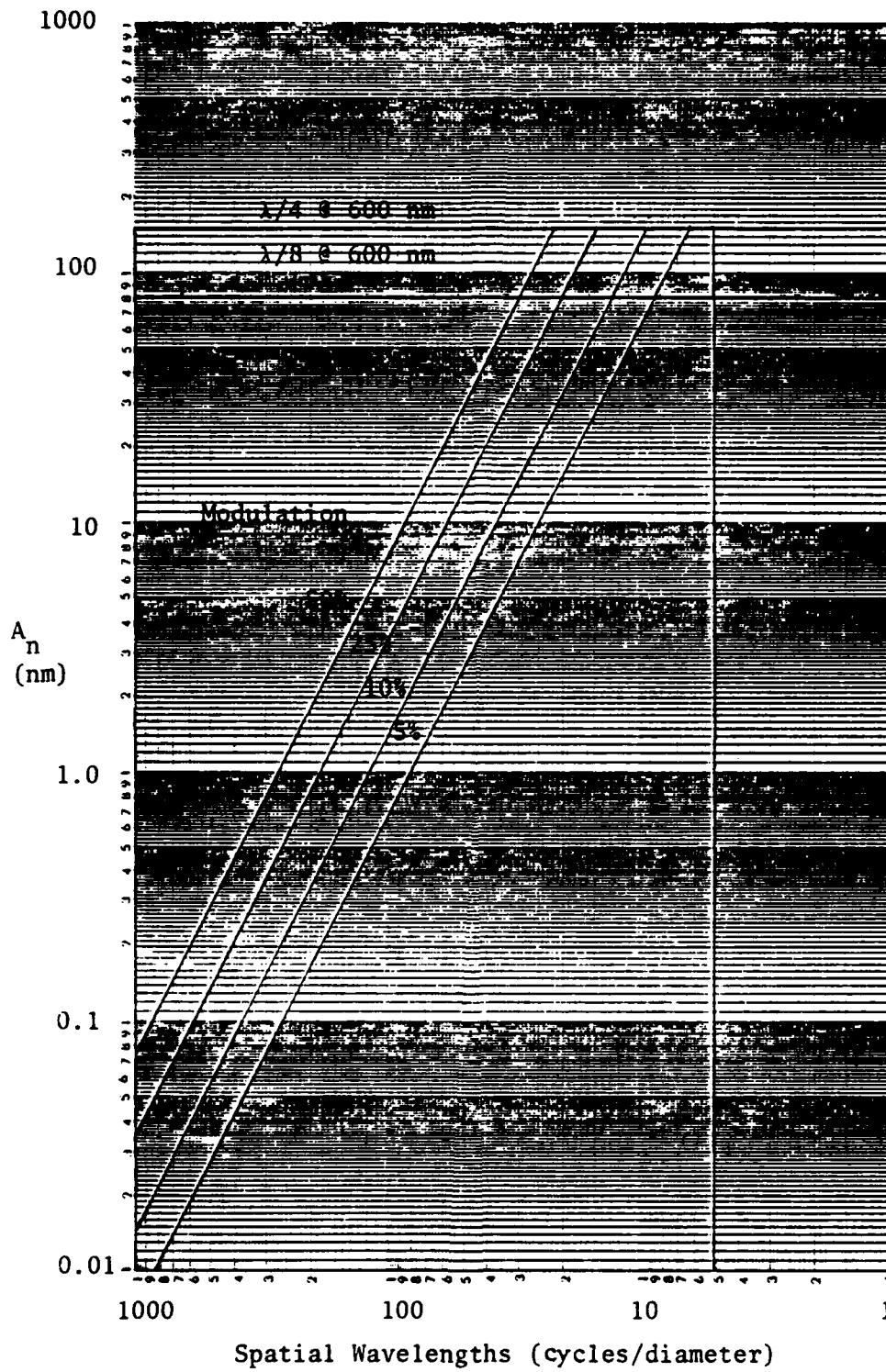
Figure 4. Detectable Amplitudes at 5% Out-of-Focus.

Errors of that amplitude in the optical surface should be fairly
obvious using interferometry.

The actual intensity modulations that would be present in the
observation plane could be less than those predicted by equation 4-2
by as much as 25 percent. This is a result of approximations made in
arriving at equation 3-14, especially the termination of the binomial
series. In spite of these approximations, the data presented in
Tables III and IV and Figures 3 and 4 indicate a large range of spatial
frequencies and surface error amplitudes that may be detectable using
the out-of-focus intensity profile. All three recording techniques
discussed earlier in this chapter (the film, fiber optic probe, and
CCD array) are capable of recording spatial frequency information
beyond the 1000 cycles per diameter boundary of the mid-range spatial
frequencies for the 10 percent out-of-focus observation plane. In the
5 percent out-of-focus case, the only method that does not quite cover
the entire range is the CCD array. These conclusions are based on the
fact that the surface error spatial frequencies expressed in cycles
per diameter are represented by the same frequencies in the out-of-
focus observation plane intensity profile since all radial quantities
scale geometrically between the optical surface and the observation
plane.

Extending this testing technique beyond this one very specific
example component requires an examination of the components optical and
testing parameters affecting the observable amplitude. The detectable error
amplitudes at a given spatial frequency are essentially independent of
the average intensity level to within the dynamic range of the detector

used. The detectable amplitudes are directly proportional to the
detectable modulation; inversely proportional to the component diameter
if all other variables are held constant; inversely proportional to
F-number holding everything else constant; and finally, out-of-focus
distance, D, as a percent of focal length is also directly proportional
to the detectable amplitudes. However, the out-of-focus parameter is
limited in available range as discussed in Chapter 3.

Some final notes on the data presented for the example component
must be made. The columns and curves presented assume a constant
detectable modulation. The actual detectors in use would generally
have detectable modulation rolloffs at higher spatial frequencies. In
addition, as the observation region becomes smaller and smaller, the
resolution limits of the various detectors will begin to close down
from the upper end of the spatial frequency spectrum. One compensating
feature in optical component testing is that as the component becomes
smaller, the spatial frequency range covered by rms surface roughness
characterization also moves toward the lower spatial frequencies.

CHAPTER 5

CONCLUSION

There is presently a gap in optical testing that leaves
approximately two orders of magnitude in the spatial frequency range,
expressed in units of cycles per diameter, untouched by currently
employed specification and testing methods. To the low side of this
mid-range spatial frequency gap lies the surface figure description
of the component. On the high spatial frequency end of the gap is
the rms surface roughness description. As the frontiers of modern
optical technology advance, this spatial frequency gap could become
a very prominent stumbling block unless methods are developed to
specify and test for these errors on an optical surface.

This research effort has isolated the spatial frequency range
that needs to be better represented by evaluating the contributions
covered by currently available testing procedures. A geometrical
analysis of an optical component was then undertaken which provided
a satisfactory explanation for a phenomenon observed in a high resolu-
tion astronomical telescope. The predictions resulting from this
geometric analysis were expanded to form the basis for a proposed
optical testing technique. This proposed testing procedure uses a
uniform plane wave source to illuminate the component being tested so
that the focused light from the component can be analyzed in an out-of-
focus observation plane located in the vicinity of the focal plane.

The intensity profile in this observation plane would provide the information needed to analyze the mid-range spatial frequency errors on the surface of the optical component. The predicted results of this type of testing hold great promise for filling a large segment of this mid-range spatial frequency gap. The predicted results section discusses the difficulty of directly correlating the intensity pattern to the amplitude of the optical surface. This presents a slight fault for the testing technique, but just knowing the spatial frequencies present and a general indication of their amplitudes could be very helpful in tracing and correcting the source of the error.

Limitations on both time and equipment availability have precluded the culmination of this research effort in an actual validation of the proposed test method. The various experimental factors involved in performing such a validation test have been discussed and the anticipated results are encouraging enough to warrant proceeding to the validation stage as soon as practical. An appropriate choice for a validation piece would be a diamond turned parabola with a known groove structure from the fabrication process. Another strong indicator of the possible utility of this testing method is the observation that the MMT displays the very effects predicted by the geometrical analysis. This research is hopefully just the first step in launching a new optical testing technique that will shed some light on the mid-range spatial frequency errors previously hidden from observation and evaluation.

APPENDIX A

BESSEL FUNCTION PROGRAM

39

TI Programmable Program Record

TITLE: Bessel Functions   PAGE 1 OF 1
PROGRAMMER: Olinger   DATE: ___
Partitioning (Op 17) |__.__| Library Module: Master Library   Printer: ___   Cards: ___

PROGRAM DESCRIPTION

Calculates Bessel Function Values to the desired number of terms of the following relations:

$$J_n(x) = \sum_{k=0}^{\infty} \frac{(-1)^k}{k!\,\Gamma(n+k+1)} \left(\frac{x}{2}\right)^{n+2k}$$

where $\Gamma(n+k+1)$ for integer values of n equals $(n+k)!$

USER INSTRUCTIONS

STEP	PROCEDURE	ENTER	PRESS	DISPLAY
1	Clear Memories		2nd CM's	
2	Initialize variable x	X	A	X
3	Initialize variable n	n	B	n
4	Initialize counter for k at -1	-1	STO 05	-1
5	Begin calculation		C	k!
6	Continue if register is not flashing		D	(n+k)!
7	Continue if register is not flashing		E	kth term
8	If k is even add to $J_n(x)$		SUM 11	
9	If k is odd substract from $J_n(x)$		INV SUM 11	
10	Repeat steps 5 through 9 to desired number of terms			
11	Obtain $J_n(x)$ from memory 11		RCL 11	

USER DEFINED KEYS	DATA REGISTERS	LABELS (Op 08)
A Store x in 10	0 master library use	0 x
B Store n in 07	1 master library use	1 $J_n(x)$
C Cal. & store n!	2 master library use	2
D Cal. & store (n+k)!	3 master library use	3
E Cal. term of $J_n(x)$	4 master library use	4
	5 k	5
	5 k!	6
	n	7
	$[k!(n+k)!]^{-1}$	8
		9
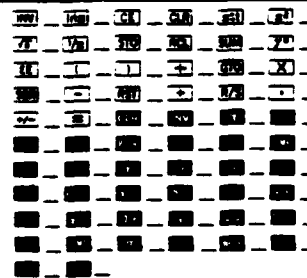
FLAGS

TITLE _____ Bessel Functions _____ PAGE _1_ OF _1_   TI Programmable

PROGRAMMER _____ Olinger _____ DATE _____   **Coding Form**

LOC	CODE	KEY	COMMENTS	LOC	CODE	KEY	COMMENTS	LOC	CODE	KEY	COMMENTS
	76	2nd Lbl		5_	54	)					
	11	A	stores x	5_	35	1/x					
	42	STO		5_	42	STO					
	10	10		5_	09	09					
	91	R/S		5_	53	(					
	76	2nd Lbl		6_	43	RCL					
	12	B	stores n	6_	10	10					
	42	STO		6_	55	÷					
	07	07		6_	02	2					
	91	R/S		6_	54	)					
1_	76	2nd Lbl		6_	45	y^k					
1_	13	C		6_	53	(					
1_	53	(		6_	43	RCL					
1_	43	RCL		6_	07	07					
1_	05	05		6_	85	+					
1_	85	+		7_	02	2					
1_	01	1		7_	65	x					
1_	54	)		7_	43	RCL					
1_	42	STO		7_	05	05					
1_	05	05		7_	54	)					
2_	36	2nd Pgm		7_	65	x					
2_	16	16		7_	43	RCL					
2_	11	A		7_	09	09					
2_	36	2nd Pgm		7_	95	=					
2_	16	16		7_	91	R/S					
2_	13	C		0_							
2_	42	STO									
2_	06	06		2_							
2_	92	INV,SBR		3_							
2_	76	2nd Lbl		4_							
3_	14	D		5_							
3_	53	(		6_							
3_	43	RCL		7_							
3_	07	07		8_							
3_	85	+		9_							
3_	43	RCL		0_							
3_	05	05									
3_	54	)		2_							
3_	36	2nd Pgm		3_							
3_	16	16		4_							
4_	11	A		5_							
4_	36	2nd Pgm		6_							
4_	16	16		7_							
4_	13	C		8_							
4_	42	STO		9_							
4_	08	08		0_							
4_	92	INV SBR									
4_	76	2nd Lbl		2_							
4_	15	E		3_							
4_	53	(		4_							
5_	43	RCL		5_							
5_	06	06		6_							
5_	65	x		7_							
5_	43	RCL		8_							
5_	08	08		9_							

TEXAS INSTRUMENTS
INCORPORATED

© 1977 Texas Instruments Incorporated

TI-24191

LIST OF REFERENCES

Beckers, J. M., and J. T. Williams. "Intensity Rings in Out-of-Focus MMT Star Images." University of Arizona, 1979.

Bennett, J. M., and J. H. Dancy. "Stylus Profiling Instrument for Measuring Statistical Properties of Smooth Optical Surfaces." Applied Optics, Volume 20, Number 10, 15 May 1981.

Born and Wolf. Principles in Optics. New York: Pergamon Press, 1965.

Church, E. L.; M. R. Howells; and T. V. Vorburger. "Spectral Analysis of the Finish of Diamond-Turned Mirror Surfaces." Unpublished and undated paper for work supported by Department of Energy and Department of Commerce.

Howes, M. T., and D. V. Morgan (eds). Charge-Coupled Devices and Systems. New York: John Wiley and Sons, 1979.

Joyce Instrumentation. Double Beam Automatic Recording Microdensitometer Mark III-C Instruction Manual. Joyce Leoble and Co., Ltd., Aug. 1963.

Kintner, Eric C., and Richard M. Sillitto. "A New Analytic Method for Computing the Optical Transfer Function." OPTICA ACTA, Volume 23, Number 8, pp. 607-619, 1976.

Kodak Publication No. P-315. Kodak Plates and Films for Scientific Photography, First Edition. Rochester NY: Eastman Kodak Company, 1973.

Levitt, M. R. (ed). Laser Focus Buyer's Guide. Newton MA: Penwell, 1982.

Loomis, John S. Fringe User's Manual, Version 2, 1976.

Malacara, Daniel (ed). Optical Shop Testing. New York: John Wiley and Sons, 1978.

Reticon Corporation. Reticon G Series Data Sheet. Sunnyvale, CA: Reticon, 1976.

END

FILMED

9-85

DTIC